Mebendazole Mesylate Monohydrate: A New Route to Improve the Solubility of Mebendazole Polymorphs

KARINA DE PAULA,[1] GERARDO E. CAMÍ,[2] ELENA V. BRUSAU,[2] GRISELDA E. NARDA,[2] JAVIER ELLENA[1]

[1]Physics Instituto of São Carlos, Universidade of São Paulo, CP 369, 13560-970, São Carlos, SP, Brazil
[2]INTEQUI-CCT-CONICET, Química Inorgánica, Departamento de Química, Facultad de Química, Bioquímica y Farmacia, Universidad Nacional de San Luis, Chacabuco 917, San Luis, 5700, Argentina

Received 15 February 2013; revised 27 May 2013; accepted 11 June 2013

Published online 29 July 2013 in Wiley Online Library (wileyonlinelibrary.com). DOI 10.1002/jps.23658

ABSTRACT: Mebendazole mesylate monohydrate, a new stable salt of mebendazole (MBZ), has been synthesized and fully characterized. It was obtained from recrystallization of MBZ forms A, B, or C in diverse solvents with the addition of methyl sulfonic acid solution. The crystal packing is first organized as a two-dimensional array consisting of rows of alternating MBZ molecules linked to columns of mesylate ions by hydrogen bonds. The three-dimensional structure is further developed by classical intermolecular interactions involving water molecules. In addition, nonclassical contacts are also found. The vibrational behavior is consistent with the crystal structure, the most important functional groups showing shifts to lower or higher frequencies in relation to the MBZ polymorphs. Thermal analysis indicates that the compound is stable up to 50°C. Decomposition occurs in five steps. Solubility studies show that the title compound presents a significant higher performance than polymorph C. © 2013 Wiley Periodicals, Inc. and the American Pharmacists Association J Pharm Sci 102:3528–3538, 2013

Keywords: mebendazole mesylate; solid state; crystal structure; FTIR–Raman spectroscopy; thermal stability; dissolution

INTRODUCTION

Mebendazole [(5-benzoyl-1H-benzimidazole-2-yl)-carbamic acid methyl ester, MBZ] is a broad-spectrum anthelmintic that demonstrated to be efficacious in the oral treatment of ascariasis, uncinariasis, oxyuriasis, and trichuriasis. It is recommended for the treatment of nonsurgical cases and as a supplementary therapy before and after surgery. Like other benzimidazole anthelmintics, MBZ primary mechanism of action is consistent with tubulin binding.[1–6]

Three polymorphic forms (A, B, and C) of MBZ displaying distinctive physical–chemical properties have been identified and characterized.[3,7,8] They have been mainly studied in relation to their thermal stability and dissolution behavior in several solvents. On the contrary, their crystal structures remained unknown up to recent times because MBZ polymorphs are usually hard to crystallize as single crystals. Lately, the complete structural data for the form C was determined by single-crystal X-ray diffraction, whereas the structure of the polymorph A was solved using synchrotron powder X-ray diffraction (PXRD) and refined by the Rietveld method.[9,10]

Regarding the solubility properties of the MBZ polymorphs, their significantly different solubility values in water condition the therapeutic effects, thus indicating the high polymorphism dependence of the anthelmintic efficacy. MBZ belongs to class II (low solubility/high permeability) of the Biopharmaceutics Classification System (BCS).

Even though some discrepancies concerning the relative solubility of forms B and C are reported in the literature, all the authors agree that form A is the most abundant and stable and then the least soluble one.[1,2,8] Thus, form C is the pharmaceutically preferred on the basis of both its stability and solubility properties even though its oral bioavailability is less than 10%.[4,6,11]

Different strategies are constantly in progress to overcome the MBZ low aqueous solubility by altering its physical properties; for example, new and better formulations that enhance the activity of the anthelmintics have been generated.[12] Another effective alternative is to interfere at the molecular level by incorporating pharmaceutically acceptable coformers into a unique crystal lattice without altering the covalent bonding of the active pharmaceutical ingredient. This approach focuses in the preparation of salts and cocrystals that are applied in the development of new dosage forms of BCS class II drugs.[13]

The crystal structures of several MBZ salts and cocrystals were also reported. Mebendazole hydrobromide was found to crystallize in a monoclinic space group, $P2_1/c$[14]; recrystallization of MBZ in propionic acid yields a 1:1 molecular complex crystallizing in the noncentrosymmetric triclinic space group, P1,[15] whereas a stable salt, mebendazole hydrochloride (orthorhombic, space group $Cmc2_1$), was also fully characterized by vibrational and thermal analyses.[16] Structural and thermal information as well as stability and dissolution studies were recently reported for some MBZ salts and cocrystals involving dicarboxylic acids as coformers.[17] Two new MBZ solvates with N,N-dimethyl acetamide (MBZ-DMA) and N,N-dimethyl formamide (MBZ-DMF) were obtained as microcrystalline forms, and other techniques such as optical and polarized microscopy, Fourier transformed infrared (FTIR) spectroscopy, thermal analysis, and PXRD were applied to their characterization.[18]

In an attempt to increase the solubility and subsequent bioavailability of not only MBZ C form but also the nonpharmaceutically preferred MBZ polymorph A, we have synthesized

Correspondence to: Griselda E. Narda (Telephone: +54-266-4424689; Fax: +54-266-4430224; E-mail: gnarda@unsl.edu.ar)

This article contains supplementary material available from the authors upon request or via the Internet at http://onlinelibrary.wiley.com/.

Journal of Pharmaceutical Sciences, Vol. 102, 3528–3538 (2013)

a new salt by incorporating a pharmaceutically acceptable coformer.

The present study reports the synthesis of mebendazole mesylate monohydrate (MBZ M) obtained from recrystallization of MBZ polymorphs A, B, or C in methyl sulfonic acid solutions. Its crystalline structure was solved by single-crystal X-ray diffraction while a complete physical–chemical characterization of the compound by solid-state techniques such as FTIR, Raman, variable-temperature FTIR (VT-FTIR), PXRD, differential thermal analysis (DTA), and thermogravimetric analysis (TGA) was also carried out. Solubility properties were investigated, and a comparative analysis taking into account MBZ polymorphs and previously reported salts is presented.

EXPERIMENTAL

Materials

All chemicals used were of analytical grade. The polymorphs A and C were kindly provided by the Laboratorio de Control de Calidad de Medicamentos, Universidad Nacional de San Luis, Argentina, whereas polymorph B was obtained by recrystallization of form C in acetonitrile. These samples were previously tested by comparing the corresponding powder X-ray diffractograms and IR spectra with those reported in the literature for the different MBZ polymorphs.

Salt Formation

A suspension containing 100 mg (0.34 mmol) of polymorph A (or B or C) and 50 mL of absolute ethanol was prepared at 25°C under stirring. Then, 0.5 mL (7.6 mmol) of methyl sulfonic acid (99.5%) was slowly added until complete dissolution of the solid. The solutions were kept about 2 weeks at 15°C, yielding colorless prismatic crystals, suitable for the crystallographic determination, in all cases. The habit of MBZ M crystals is shown in Figure S1 (see Supporting Information). As it can be seen, the single crystals show a highly breakable needle shape.

In addition, all polymorphs yielded a polycrystalline form by dissolution in other organic solvents such as acetonitrile or methanol with further addition of methyl sulfonic acid solution. The obtained products were filtered, washed with a hexane–ethanol mixture (20:1), and dried under room conditions for further characterization.

Methods

A suitable-sized clear crystal was selected for the single-crystal X-ray diffraction experiment. Intensity data were measured at room temperature (RT) (293 K) with MoKα radiation (λ = 0.71073 Å) from a graphite monochromator, using an Enraf-Nonius Kappa-CCD diffractometer (Enraf-Nonius, Delft, The Netherlands).

Crystal detector distance was fixed at 40 mm, and a total of 346 images were collected using the oscillation method, with scan angle by frame 2° oscillation and 120 s exposure time by image. Data collection strategy was calculated with the program collect.[19] Data reduction and cell refinement were performed with the software HKL Denzo and Scalepack.[20] Tables were generated by WinGX,[21] ORTEP-3,[22] MERCURY,[23] enCIFer,[24] and PLATON[25] programs were employed to prepare material for publication.

The crystal structure was solved by direct methods using the program SIR-97.[26] Anisotropic least-squares refinement was carried out with SHELXL-97.[27] All non-hydrogen atoms were anisotropically refined. The C–H hydrogen atoms were stereochemically positioned, and were refined with fixed individual displacement parameters [Uiso (H) = 1.2 Ueq(Csp^2) or 1.5 U eq (Csp^3)] using a riding model with aromatic C–H bond length of 0.93 Å. The N-bound H atom was located by difference Fourier synthesis, and its position was fixed as initially found, with U iso (H) = 1.2 U eq (N). Geometrical calculations were carried out with PARST.[28,29] Table 1 summarizes the structural and refinement parameters of MBZ M.

The analysis of the intramolecular geometrical parameters of MBZ in the salt was performed with MOGUL[31] by applying the following filters: R factor less than 5% and the exclusion of metal-organic compounds. This program was developed in 2004 and includes structural information that gives quick access to values of bond lengths, valence, and torsion angles of structures with similar geometries and molecular conformation, deposited in the Cambridge Structural Database (CSD),[32] which contains the results of 600,000 (up to January 2012) crystal-structure determinations of organic and metal-organic compounds.

The crystallographic information file (CIF) loading the data sets (excluding the structure factors) for MBZ M has been deposited with the CSD under deposit code CCDC 934635 (copies of these data may be obtained free of charge from The Director, CCDC, Cambridge CB2 1EZ, UK, Fax: +44-123-336-033; E-mail: deposit@ccdc.cam.ac.uk or http:www.ccdc.cam.ac.uk).

Powder X-ray diffraction diagrams were obtained with a Rigaku D-MAX-IIIC diffractometer (Rigaku Company, Tokyo, Japan) using CuKα radiation (Ni filter) and NaCl and quartz as external calibration standards.

Fourier transformed infrared spectra were recorded on a Nicolet Protégé 460 spectrometer (Nicolet Instrument Corporation, Madison, Wisconsin) provided with a CsI beamsplitter in the 4000 –225 cm^{-1} range with 32 scans and spectral resolution of 4 cm^{-1}, using the KBr pellet technique. The spectra at controlled increasing temperatures were recorded by placing the pellet in a variable-temperature IR cell in the range 25°C–250°C. The Raman spectrum was obtained with a Bruker 66 spectrophotometer (Bruker Corporation, MA) provided with the FRA 106 Bruker accessory, using 1064 nm excitation line.

Thermogravimetric analysis and DTA curves were obtained with Shimadzu TGA-51 and DTA-50 thermal analyzers (Shimadzu Inc., Kyoto, Japan), using platinum pans, flowing air at 50 mL min^{-1}, and a heating rate of 10°C min^{-1} from RT to 1000°C.

Solubility Determination

The dissolution experiments for MBZ polymorphs A and C as reference drugs, and both salts (MBZ M and MBZ·HCl) were conducted under nonsink conditions and without surfactant addition. This is considered as the most appropriate approach in developing a biorelevant dissolution method for a poorly water-soluble drug such as MBZ.[33–35] For obtaining the dissolution profiles, an amount of 200 mg of MBZ M, MBZ A, MBZ C, and MBZ·HCl was compressed at a pressure of 300 kg cm^{-2} for 5 min using a hydraulic press into disks of 13.1 mm diameter and 1.15 mm thickness. The disks were suspended in 500 mL of pH 1 dissolution medium (0.1 M HCl solution) at 37°C using a Hanson SR8 dissolution equipment (Hanson Corporation, CA) with paddles rotating at 120 rpm, which allows smoothly stirring conditions without significant wobble (Method 2 of the

Table 1. Crystal Data and Structure Refinement for MBZ M

Empirical formula	$C_{17}H_{19}N_3O_7S$	
Temperature (K)	293(2)	
Formula weight (g.mol^{-1})	409.41	
Wavelength (Å)	0.71073	
Crystal system	Triclinic	
Space group	$P\bar{1}$	
Unit cell dimensions (Å; °)	$a = 6.8339(2)$	$\alpha = 86.948(2)$
	$b = 9.3030(3)$	$\beta = 86.577(2)$
	$c = 14.6869(4)$	$\gamma = 80.693(2)$
Volume (Å^3)	918.89(5)	
Z	2	
Density (calculated) (mg/m^3)	1.480	
Absorption coefficient (mm^{-1})	0.223	
F(000)	428	
Crystal size (mm)	0.73 × 0.14 × 0.11	
Theta range for data collection	3.02°–27.48°	
Index ranges	$-8 \le h \le 8$, $-11 \le k \le 11$, $-19 \le l \le 18$	
Collected Reflections	7568	
Independent reflections	4137 [$R_{int} = 0.0287$]	
Completeness to theta = 27.48°	98.5%	
Refinement method	Full-matrix least squares on F^2	
Absorption correction	Gaussian [30]	
Data/restraints/parameters	4137/0/255	
Goodness-of-fit on F^2	1.066	
Final R indices [$I > 2\sigma(I)$]	R1 = 0.0537, wR2 = 0.1439	
R indices (all data)	R1 = 0.0689, wR2 = 0.1569	
Largest difference peak and hole (e. Å^{-3})	0.284 and −0.525	

USP 29, modified).[1,36] Samples were taken every 5 min during the first 75 min, then every 15 min up to 120 min, and finally, the sampling time was 60 min in the range 120 –780 min.

Intrinsic dissolution rate experiments were conducted in a rotating disk apparatus under the same experimental conditions by using disks prepared as described previously. The absorbance measurements at 283 nm for each sample were performed with a Shimadzu UV–Vis 1603 (Shimadzu Inc.). The absorbance values were converted into solution concentration ones by means of a calibration curve for MBZ (Fig. S2, Supporting Information). Experimental results were the average of five replicated experiments.

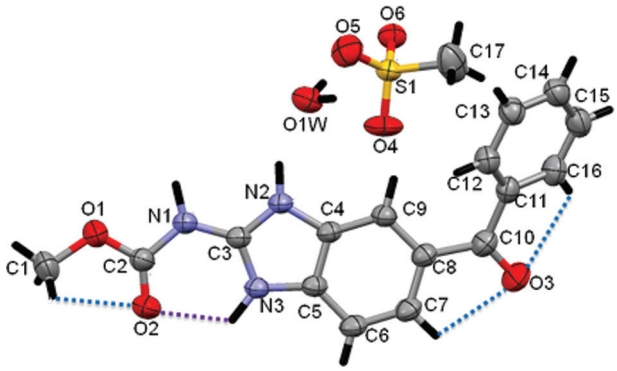

Figure 1. ORTEP–3 view of the asymmetric unit of MBZ M showing the atoms labeling, the 50% probability ellipsoids, and the intramolecular interactions. Nonclassical interactions are indicated in blue dashed lines.

RESULTS AND DISCUSSION

Crystal Structure

The experimental PXRD diagram can be satisfactorily compared with the theoretical one obtained by simulation with MERCURY[23] inputting the MBZ M CIF file created after the structural refinement (see Fig. S3, Supporting Information). In addition, PXRD patterns and FTIR spectra of the crystalline powders confirmed that different solvents render the same salt of MBZ.

Figure 1 shows an ORTEP-3[22] view of the asymmetric unit of MBZ M, which contains one MBZ molecule, one mesylate ion, and one water molecule. The MBZ M presents the azolic nitrogen located on N(3), unlike other compounds, such as MBZ·HCl, where the azolic nitrogen is positioned on N(2).[16]

The analysis of the molecular conformation reveals classical and nonclassical intramolecular hydrogen bonds whose respective distances and angles are shown in Table 2.

Table 2. Geometrical Parameters of the Intramolecular Interactions (with estimated standard deviations in Parenthesis)

D–H•••A	D–H (Å)	D•••A (Å)	H•••A (Å)	D–H•••A (°)
N(3)–H(3)•••O(2)	0.990	2.724(2)	2.117	117.76(9)
C(1)–H(1c)•••O(2)	0.960	2.680(3)	2.565	86.30(13)
C(7)–H(7)•••O(3)	0.930	2.758(3)	2.440	99.99(13)
C(16)–H(16)•••O(3)	0.930	2.802(3)	2.542	96.35(14)

The classical intramolecular hydrogen bond [N(3)–H(3)•••O(2)] between the carbonyl of the carbamate group and the nitrogen atom N3 of the heterocycle closes a chelating six-membered system. This H-bond is stabilized by a resonance effect involving the atoms H(3)–N(3)–C(3)–N(1)–C(2)–O(2). This electron delocalization

 DOI 10.1002/jps.23658

Table 3. Bond Length Values Involved in the Resonance-Assisted Hydrogen Bond Compared with the Respective Values Obtained by MOGUL[31] (with estimated standard deviations in Parenthesis)

Fragment	Bond Length (Å)	Average Value (Å)
N(3)–C(3)	1.341(2)	1.349
C(3)–N(1)	1.355(2)	1.336
N(1)–C(2)	1.381(2)	1.374
C(2)–O(2)	1.195(2)	1.211

effect is called resonance-assisted hydrogen bond (RAHB),[37,38] and is characterized by an interaction between a hydrogen atom connected to an electronegative atom (N or NH) and to another electronegative atom of the same molecule (=O) connected to a π-conjugated system (O=C–C=C–OH, O=C–C=C–NH, or O=C–N=C–NH). This electron delocalization effect is of great importance for the stabilization of the intramolecular interaction (RAHB effect). This resonant effect influences the bond lengths of the atoms involved as can be seen from the N(3)–C(3) and C(2)–O(2) bond distances that get shorter, whereas the C(3)–N(1) and N(1)–C(2) ones become longer than the mean value for this kind of compounds. Table 3 displays the bond length values involved in the hybrid resonance according to the program MOGUL.[31] The highest deviation from the least-squares plane passing through the above-mentioned six cyclic atoms is − 0.0113(5) Å (root mean square deviation).

The crystal structure presents a three-dimensional packing stabilized by classical and nonclassical intermolecular interactions. The different interactions originate hydrophilic channels in which the mesylate ions and water molecules are distributed (Fig. 2a). The packing consists of rows of alternating MBZ molecules linked through hydrogen bonds to columns of mesylate ions (Fig. 2b).

Each molecule of MBZ participates in three intermolecular interactions, all of them belonging to the N–H•••O type, two of them to mesylate ions, and the remaining one to a water molecule. No classical intermolecular interactions are found between MBZ molecules. Furthermore, each mesylate group participates in four intermolecular interactions involving two MBZ and two water molecules. Finally, each water molecule participates in three intermolecular interactions, two of them involving two mesylate groups and the remaining one with a MBZ molecule (Fig. 3).

The N(1)–H(1)•••O(6) hydrogen bond connects the nitrogen of the carbamate group with the oxygen of the mesylate ion. Furthermore, the nitrogen N(3) of the benzimidazole group is also hydrogen bonded to the O(4) from another mesylate ion. This same oxygen atom also acts as an acceptor in a nonclassical intermolecular interaction with a carbon atom of the benzimidazole group, C(6)–H(6)•••O(4). These three mentioned intermolecular interactions lead to the formation of infinite chains along the *b* axis (Fig. 4, Table 4). These chains form two-dimensional arrays in which successive chains are rotated 180° along the *b* axis, which places the phenyl groups of a chain toward the corresponding ones belonging to the adjacent chain. These two-dimensional arrays are linked together through intermolecular interactions involving water molecules allowing the development of the three-dimensional packing. Thus, each mesylate ion interacts with two different water molecules through strong hydrogen bonds O(1w)–H(11W)•••O(5) and O(1w)–H(12w)•••O(6). In turn, water molecules behave as acceptors for other classical hydrogen bonds involving the nitrogen atom N(2) from the benzimidazole group, N(2)–H(2)•••O(1w).

As it was already mentioned, π−π stacking interactions are also present in the crystal packing of MBZ M. In this type of interaction, the rings are arranged so as to position themselves parallel to each other but exhibiting an offset of their centroids in the ring plane, thus leading to a decrease in the electron repulsion. Although weak, these interactions represent a significant contribution to the aggregate of molecules that form a crystal, thereby decreasing the crystalline energy. In the π−π stacking interactions, the centroids are separated by 3.743 Å, with a displacement between centroids of 26.33° (Fig. S4, Supporting Information).

Statistical Analysis of Molecular Parameters

The analysis of the MBZ M geometrical parameters performed with the MOGUL program[31] shows important deviations for several parameters when compared with the expected values (see Table 5). The major disagreements involve the C(7)–C(8) and O(2)=C(2) bond lengths. The difference found in the former

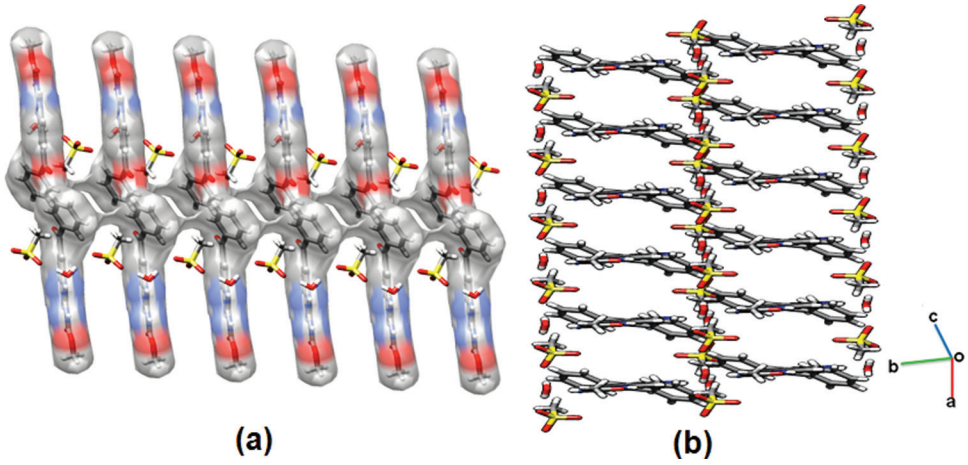

Figure 2. (a) MBZ M crystal packing showing the hydrophilic channels containing the mesylate ions and water molecules; (b) view of the rows interspersed by MBZ and mesylate ions along the [100] direction.

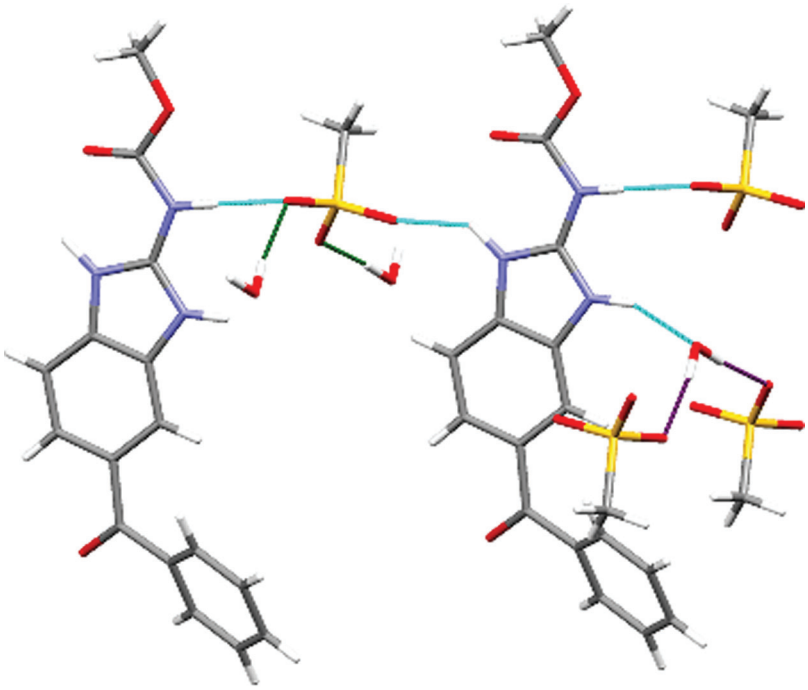

Figure 3. Classical intermolecular interactions in the MBZ M crystal structure.

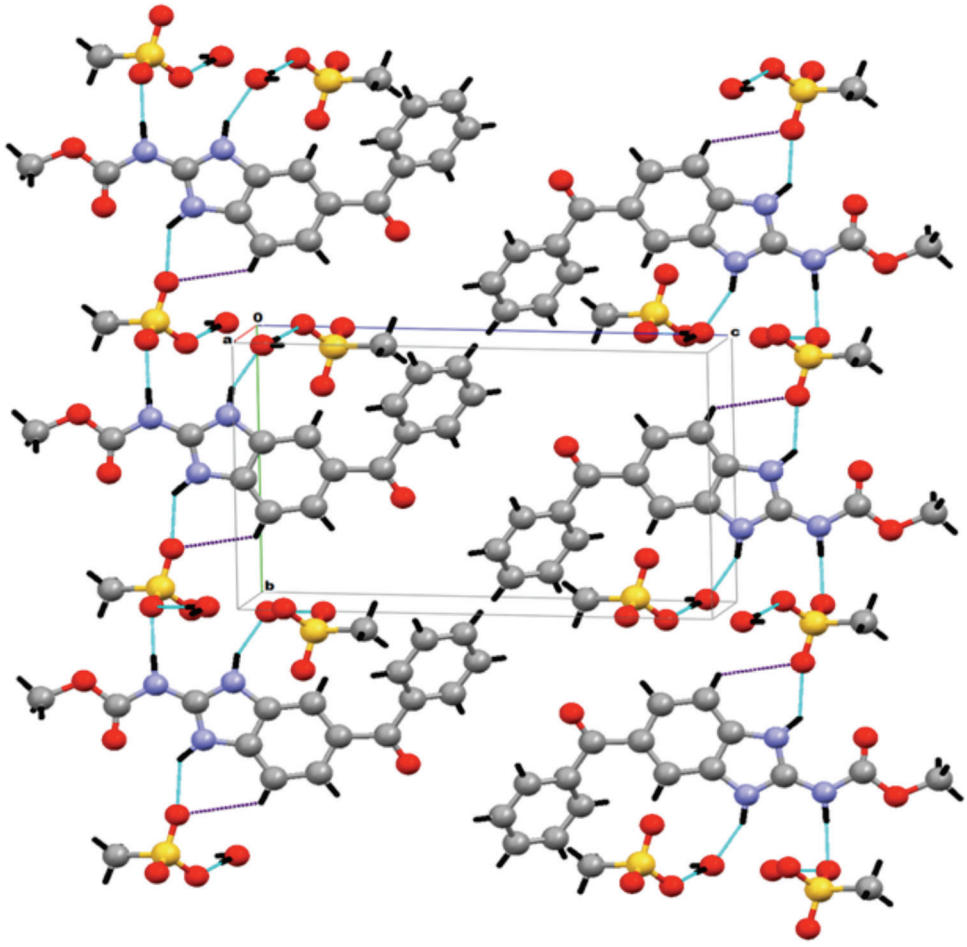

Figure 4. Intermolecular interactions in MBZ M along the [010] direction. Classical intermolecular interactions are outlined in blue lines and the nonclassical ones in purple.

 DOI 10.1002/jps.23658

Table 4. Selected Intermolecular Interactions Parameters (with estimated standard deviations in Parenthesis)

D–H•••A	D–H (Å)	D•••A (Å)	H•••A (Å)	D–H•••A (°)
N(2)–H(2)•••O1w[a]	0.951	2.679(2)	1.785	155.3(1)
O(1w)–H(11w)•••O(5)[b]	0.955	2.776(2)	1.823	175.9(1)
N(1)–H(1)•••O(6)[a]	0.984	2.728(2)	1.744	177.7(1)
N(3)–H(3)•••O(4)[b]	0.990	2.755(2)	1.959	135.6(1)
O(1w)–H(12w)•••O(6)[c]	0.820	2.879(2)	2.076	166.2(1)
C(6)–H(6)•••O(4)[b]	0.930	3.227(3)	2.614	123.9(1)

Symmetry operations: [a] $-x+1,-y,-z$; [b] $-x+1,-y+1,-z$; [c] $x+1,y,z$.

one is a consequence of the participation of the C(7) in the intramolecular interaction with oxygen O(3), as previously described. The difference in the second bond length is because of the presence of the resonance-assisted interaction involving atoms H(3)–N(3)–C(3)–N(1)–C(2)–O(2). This effect leads to a redistribution of the electron charge density that decreases the O(2)=C(2) bond length, when compared with the average value. The other bonds that are also involved in resonance show similar deviations.

Figure 5 depicts the histograms for the O3–C10 bond distance and the O3–C10–C11 bond angle as well as for the O3–C10–C8–C9 torsion angle. It is worthy to note that for the torsion angle, there are two preferred values for the same fragment. These parameters were chosen because they all lie in the region of the phenyl and benzimidazole groups, that is, in a region where the oxygen atom participates in two intramolecular interactions of the C–H•••O type, these interactions being responsible for the stabilization of the phenyl ring conformation. Thus, these interactions lead to an increase in the O3–C10 bond length and to a contraction in the O3–C10–C11 valence angle.

Comparison with Others Solid Forms of MBZ

Figure 6 shows the overlap of the MBZ moiety in the MBZ M molecule with the corresponding one in the other MBZ solid forms reported by us. The overlap of the molecular conformations indicates that the main differences involve the phenyl ring and the carbamate group. In all of them, the carbamate group is coplanar with the benzimidazole ring (within experimental error). For MBZ·HCl, a satisfactory overlap was not possible to obtain because of the particular molecular conformation of the MBZ related to the conformational σ (Sigma) binding between nitrogen and oxygen of the carbamate group. In MBZ M, methoxy and benzoyl group are in a *trans*-conformation, whereas in MBZ·HCl, they adopt a *cis*-conformation.[16] These differences in the conformation of the carbamate group are characterized by rotations about the C(2)–N(1) and N(1)–C(3) bonds.

Vibrational Spectra

The FTIR and Raman spectra of MBZ M are presented in Figures S5 and S6 (see Supporting Information), respectively. VT-FTIR spectra are gathered in Figure S7 (see Supporting Information). Table 6 shows the assignment of the vibrational modes performed on the basis of the most important functional groups such as carbonyl, NH, CN, SO, and OH. The main differences among the vibrational behavior of MBZ polymorphs, MBZ·HCl and MBZ M are also analyzed.

NH and OH Modes

Three intense bands at 3475, 3370, and 3210 cm^{-1} are identified in the high-frequency region in the MBZ M spectrum. The relatively broad band at 3210 cm^{-1} is assigned to the N–H stretching mode. For MBZ·HCl, the νN–H bands are observed at 3216 and 3144 cm^{-1}, the last one being associated to the N_{azolic}–H(HCl). The considerably stronger hydrogen bonds derived from the basicity of the mesylate and chloride anions could explain the shifting to lower frequencies of this mode when comparing with the MBZ polymorphs.[1,5]

The bands centered at 3475 and 3370 cm^{-1} are assigned to the νO–H mode of crystallization water. This assignment is justified by their disappearance in the VT-FTIR spectra at temperatures consistent with dehydration (Fig. S7, Supporting Information).

The imine and carbamate NH bending modes occur in the IR and Raman spectra at 1650, 1635, and 1600 cm^{-1}. Furthermore, the band at 1650 cm^{-1} presents another component associated

Table 5. Selected Disagreement Values for Bond Lengths (Å) and Angles (°) Obtained with the MOGUL Program

	Value in Query	Statistics Total	Mean	Median	Standard Deviation	l *z–Score* l
Bond						
C7–C8	1.406	2417	1.389	1.390	0.011	1.536
O2–C2	1.195	1373	1.211	1.212	0.011	1.510
C11–C10	1.501	450	1.490	1.491	0.010	1.183
O3–C10	1.226	960	1.227	1.223	0.014	0.044
Torsion angle						
C6–C7–C8	122.775	2684	120.791	120.771	0.951	2.086
C7–C6–C5	116.203	744	120.054	120.640	1.798	2.142
C7–C8–C10	116.949	714	120.577	120.767	1.993	1.821
C16–C11–C10	117.436	714	120.577	120.767	1.993	1.576
C12–C11–C10	123.627	714	120.577	120.767	1.993	1.530
O3–C10–C11	118.351	450	119.878	119.945	1.520	1.004

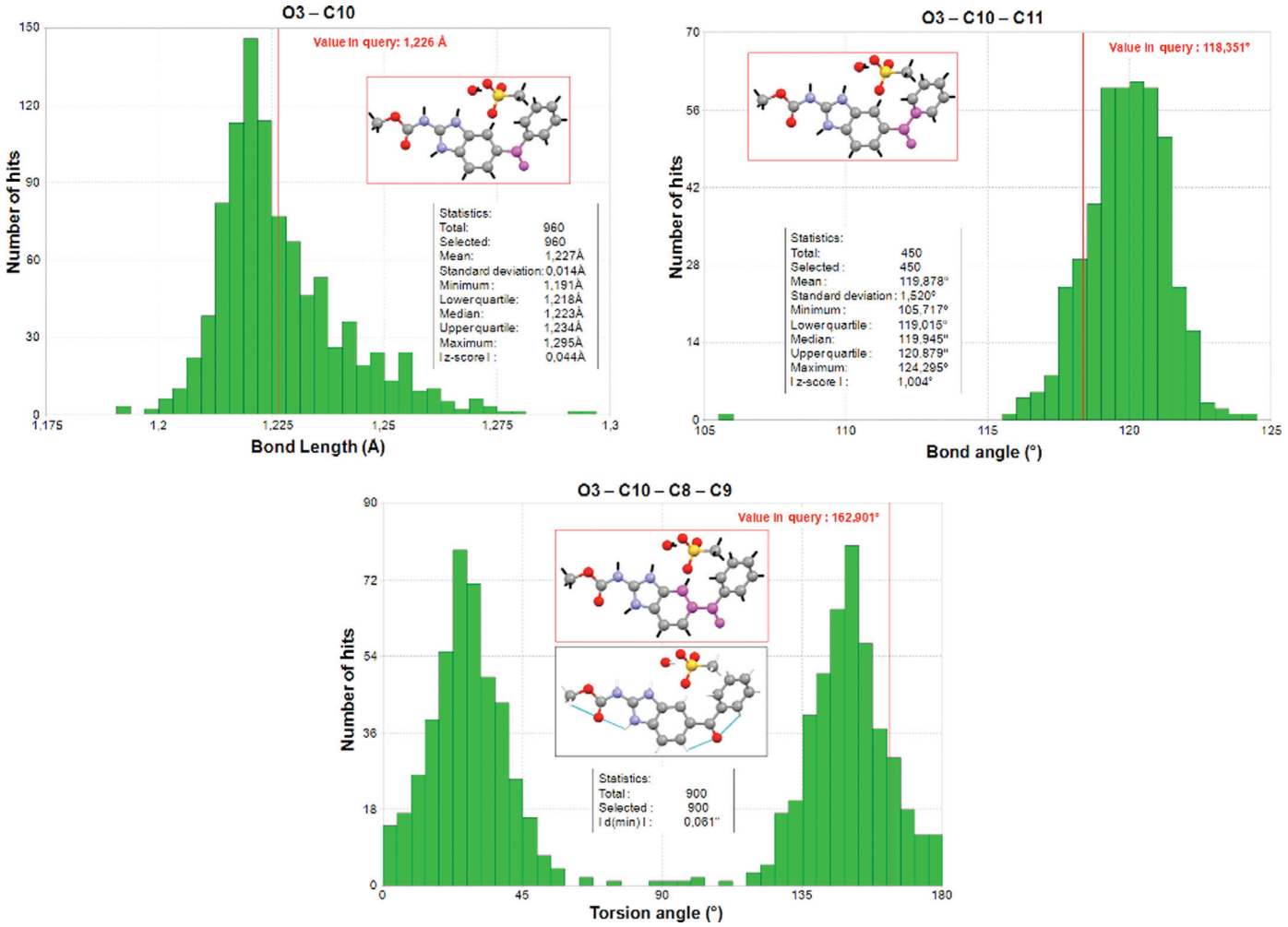

Figure 5. Histograms obtained by the MOGUL program for (a) O3–C10 bond length, (b) O3–C10–C11 bond angle, and (c) O3–C10–C8–C9 torsion angle.

with the $\nu C{=}O_{(ketonic)}$ mode, whereas the band at 1600 cm^{-1} involves the δH_2O mode because it is progressively modified when temperature raises from RT to 150°C.

CO Modes

Both carbonyl groups in MBZ M are involved in two intramolecular H-bonds each one. The IR and Raman spectra exhibit the characteristic band of the $\nu C{=}O_{(carbamic)}$ mode at 1750 cm^{-1}. Polymorphs A, B and C present this mode at 1730, 1720, and 1700 cm^{-1}, respectively;[1,5] for MBZ·HCl it is observed at 1767 cm^{-1} (IR) and 1760 cm^{-1} (Raman).[16]

The bands at 1365 cm^{-1} (IR) and 1370 cm^{-1} (Raman) have been attributed to the C–O–C stretching mode in accordance with the reference values.[39–41]

CN Modes

The νC–N mode is identified at 1635 cm^{-1} overlapped with the δN–H mode, both in IR and Raman spectra, and at 1565 cm^{-1}.

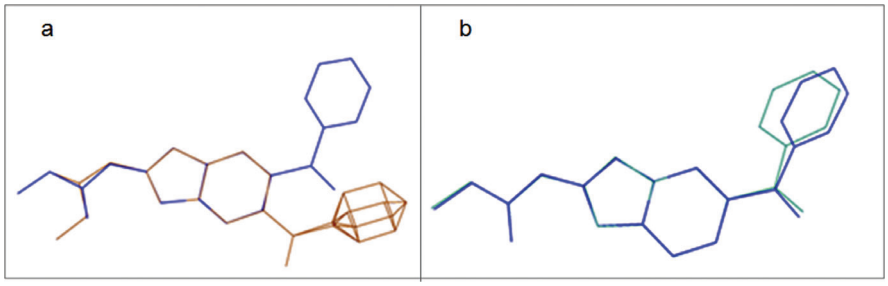

Figure 6. Superposition of the MBZ moiety of the different MBZ solid forms reported by us in the literature (MBZ M in blue): (a) MBZ·HCl (orange) and (b) form C (green).

DOI 10.1002/jps.23658

Table 6. Selected Vibrational Modes of the Raman and FTIR Spectra of MBZ M

Mode	FTIR Wavenumbers (cm^{-1})	Raman Wavenumbers (cm^{-1})
νOH (water)	3475 (m), 3370 (m)	
νNH Modes	3210 (m)	
δNH + νC = O (ketone)	1650 (s)	
δNH + νCN	1635 (w)	1650 (sh)
δNH + δH_2O	1600 (m)	1635 (m)
νCN	1565 (m), 1505 (w)	1599 (m) 1565 (w), 1500 (vw)
νC = O (carbamate)	1750 (s)	
νC–O–C	1370 (w)	1750 (w)
νC–C	1290 (w)	1369 (m)
SO Modes		
ν_{as}SO	1240 (s), 1155 (s)	
ν_sSO	1040 (s)	1240 (w), 1150 (w)
νCH (aromatic)	3100 (m), 3070 (m), 3060 (m)	1050 (w)
		3099 (vw), 3074 (w), 3064 (sh), 3011
νCH (aliphatic)	2955 (m)	(vw)

s, Strong; m, media; w, weak; vw, very weak; sh, shoulder; d, doublet; ν, stretching; δ, deformation; ρ, rocking; s, symmetric; as, antisymmetric.

The higher frequency band could be assigned to the C=N bond of the benzimidazole ring; this band is shifted to lower frequency regarding the corresponding C=N frequency values[39–41] and reveals losing of the double bond character in the benzimidazole ring. The lower frequency band is associated with the carbamate C–N simple bond.

Thermal Studies

Figure 7 displays the TGA and DTA curves for MBZ M. The proposed thermal decomposition of the compound is shown in Scheme 1.

An analysis of the thermal data indicates that MBZ M degradation occurs in five steps. The first stage involves a mass decay of 4.6% (calculated: 4.4%, onset: 50°C) associated with an endothermic DTA signal. This fact was confirmed by the VT-FTIR spectra (Fig. S7, Supporting Information) that show the disappearance of the bands derived from water molecules. The corresponding anhydrous compound remains stable up to 150°C without undergoing through phase transitions or melting process. The second step is also endothermic in nature and accounts for the breakdown of the carbamate moiety[16] with further elimination of CO_2, the weight loss being 16.1% (calculated: 14.17%, onset: 215°C). This fact is supported by the absence of the IR bands located at 1750 and 3210 cm^{-1} in the spectrum recorded at 200°C (Fig. S7, Supporting Information).

The following three mass decays consist of successive events with no stability plateau among them; the first two stages of –27.6% (calculated: –25.67%; onset 330°C and 400°C) are associated with relatively weak and complex DTA signals. In an attempt to elucidate these processes, a small amount of sample was heated at 400°C and then, the corresponding FTIR spectrum was recorded. The decrease in the intensity of the 1650 cm^{-1} band and the disappearance of high- and medium-frequency bands assigned to the C–H modes are observed. These evidences suggest the elimination of the benzoyl moiety. The final step involves a 51.7% weight loss (calculated: 55.51%; onset 450°C) accompanied with an important exothermic signal, resulting in the complete decomposition of the compound.

The thermal evolution of MBZ M is substantially different from those of MBZ·HCl[16] or MBZ polymorphs[8]; the presence of a coformer with high thermal stability could explain this observation.

Solubility Studies

Solubility at a defined temperature and pressure is the saturation concentration of the dissolved drug in equilibrium with the solid drug. Aqueous solubility of drugs is traditionally determined using the equilibrium solubility method that involved

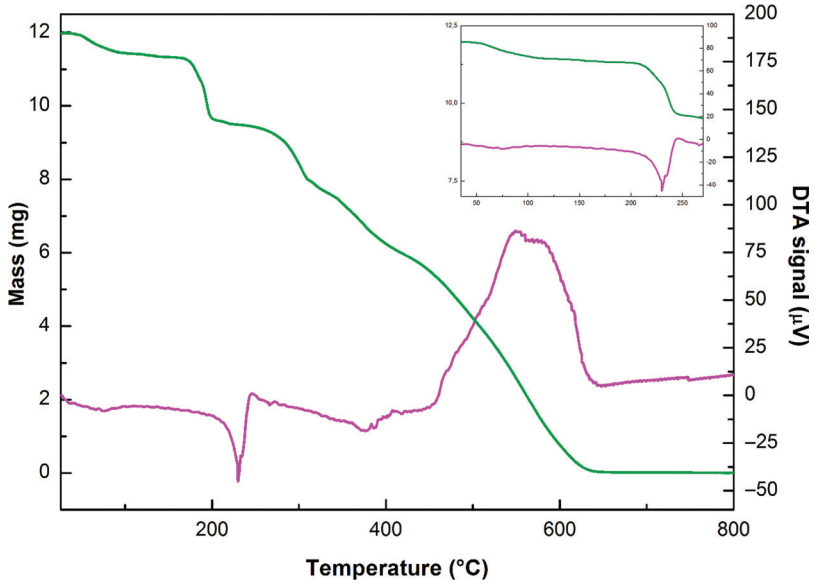

Figure 7. TGA and DTA curves for MBZ M. (Inset) Zoom in the RT to 270°C range.

suspending an excess amount of a solid drug in a selected aqueous medium.

The dissolution profiles in comparison with those of MBZ polymorphs A and C and MBZ·HCl are shown in Figure 8a, whereas the intrinsic dissolution rate curves are displayed in Figure 8b.

The maximum solubility values for the forms A and C and both salts are given in Supporting Information (Table S1). These values indicate that MBZ M is 3.1 and 19.2 times as large as that of polymorphs C and A, respectively, whereas MBZ·HCl is 1.2 times more soluble than MBZ M.

Both salts exhibit an important increase in solubility and dissolution rate as compared with MBZ forms A and C; in addition, they are even more soluble than the MBZ-oxalate monohydrate and the MBZ-maleate salts reported by Chen et al.,[17] with reference to the corresponding form C solubility values in all cases.

The maintenance of the initial form for each compound assayed was confirmed at the end of the dissolution experiments by FTIR spectrometry, showing that no solution-mediated transformation was observed during the reported period.

The solubility profiles are promising because higher concentration of the drug can be achieved at a faster rate through salt formation.

CONCLUSIONS

The use of methyl sulfonic acid as a coformer leads to a new MBZ salt, which is able to improve significantly the poor MBZ solubility. The crystal structure of a new salt, MBZ M, shows a two-dimensional array consisting of MBZ molecules and mesylate ions with further development of the three-dimensional packing via intermolecular H-bonds involving the water molecules. Other weak interactions also contribute to the solid-phase stabilization. Unlike other MBZ solid forms, MBZ M presents a rich intramolecular interactions pattern with formation of four rings, one of them being stabilized by the RAHB effect that affects the involved bond distances. The vibrational behavior is consistent with the structural findings. Thermal studies indicate that the salt dehydrates at 50°C and further continues its thermal evolution without converting to any solid form of MBZ because of the high stability of the mesylate moiety on heating. Finally, solubility experiments at pH 1 demonstrated that MBZ M exhibits a much better performance than MBZ polymorphs A and C.

ACKNOWLEDGMENTS

The authors thank the Brazilian agencies CNPq, CAPES, and FAPESP and Argentinian ones CONICET (PIP 2008-01360) and SECyT-UNSL for financial support. G.E.N. is a member of the CONICET.

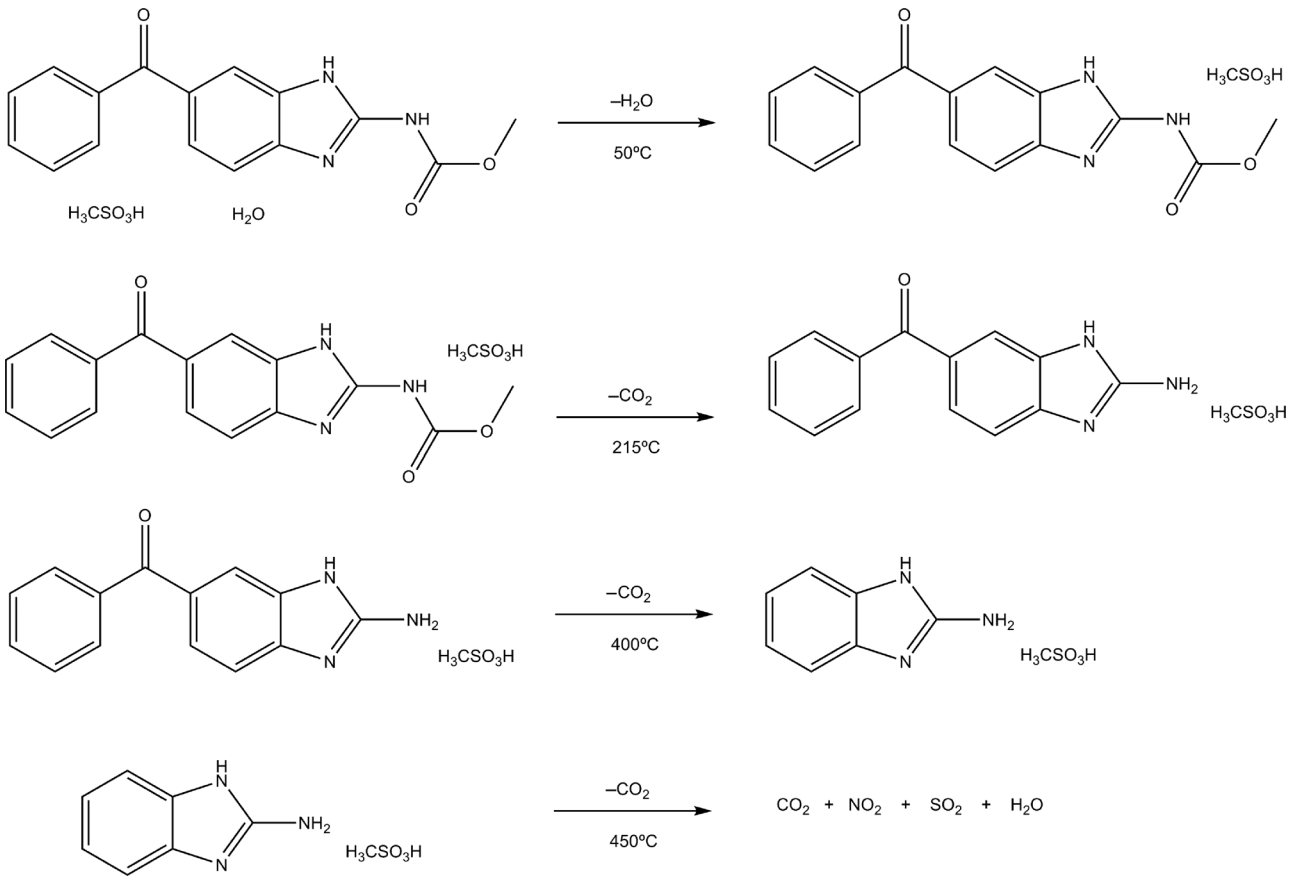

Scheme 1. Proposed thermal degradation of MBZ M.

 DOI 10.1002/jps.23658

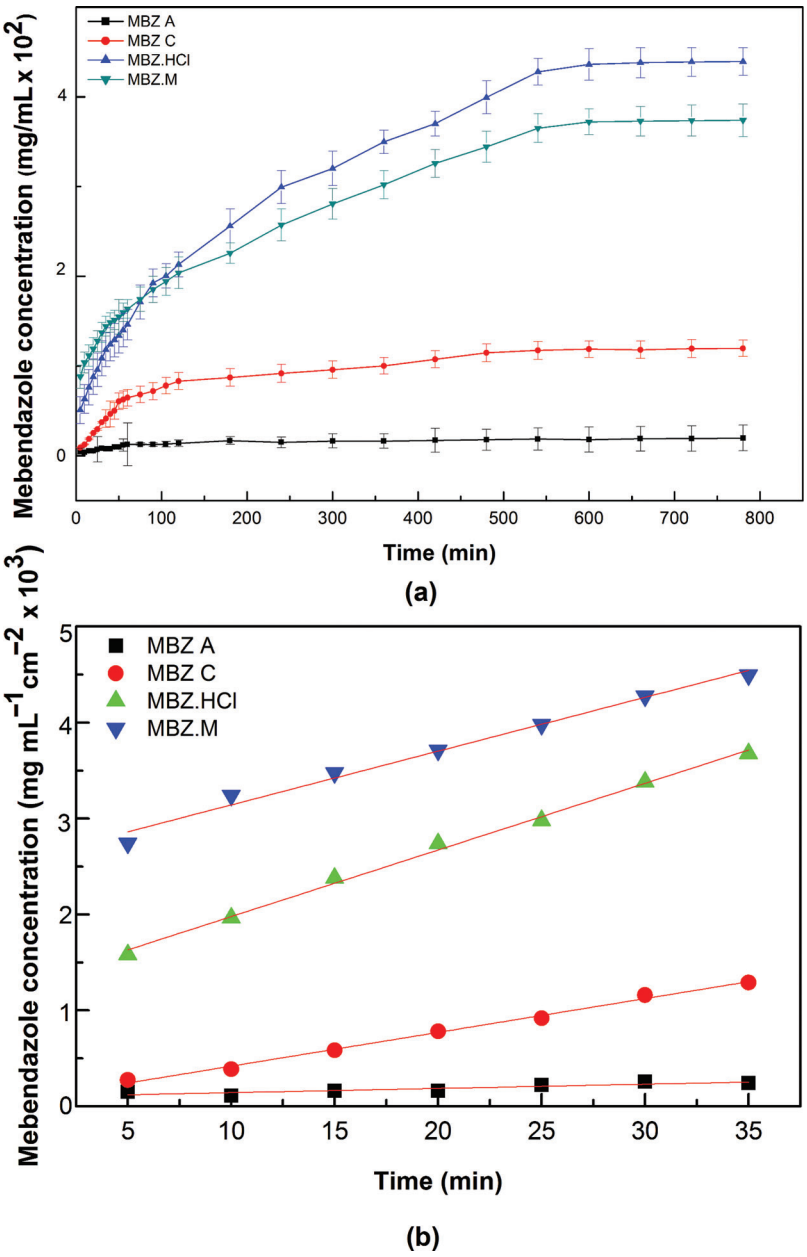

Figure 8. Dissolution profiles of MBZ M in comparison with those of MBZ polymorphs A and C and MBZ·HCl for (a) 780 min and (b) 35 min. Intrinsic dissolution rates (mg mL^{-1} min^{-1} cm^{-2}): A, 4.4×10^{-6} ($R^2 = 0.8$); C, 3.5×10^{-5} ($R^2 = 0.99$); MBZ·HCl, 6.94×10^{-5} ($R^2 = 0.99$); MBZ M 5.6×10^{-5} ($R^2 = 0.98$).

REFERENCES

1. Swanepoel E, Liebenberg W, de Villiers MM. 2003. Quality evaluation of generic drugs by dissolution test: Changing the USP dissolution medium to distinguish between active and non-active mebendazole polymorphs. Eur J Pharm Biopharm 55:345–349.

2. Swanepoel E, Liebenberg W, Devarakonda B, de Villiers MM. 2003. Developing a discriminating dissolution test for three mebendazole polymorphs based on solubility differences. Pharmazie 58:117–121.

3. Liebenberg W, Dekker TG, Lotter AP, de Villiers MM. 1998. Identification of mebendazole polymorphic form present in raw materials and tablets available in South Africa. Drug Dev Ind Pharm 24:485–488.

4. Charoenlarp P, Waikagul J, Muennoo C, Srinophakun S, Kitayaporn D. 1993. Efficacy of single-dose mebendazole, polymorphic forms A and C, in the treatment of hookworm and T*richuris* infections. Southeast Asian J Trop Med Public Health 24:712–716.

5. Costa J, Fresno M, Guzmán L, Igual A, Oliva J, Vidal P, Pérez A, Pujol M. 1991. Polymorphic forms of mebendazole: Analytical aspects and toxicity. Circ Farm 49:415–424.

6. Agatonovic-Kustrin S, Glass BD, Mangan M, Smithson J. 2008. Analysing the crystal purity of mebendazole raw material and its stability in a suspension formulation. Int J Pharm 361:245–250.

7. Himmelreich M, Rawson BJ, Watson TR. 1977. Polymorphic forms of mebendazole. Aust J Pharm Sci 6:123–125.

8. Rodriguez-Caabeiro F, Criado-Fornelio A, Jimenez-Gonzalez A, Guzmán L, Igual A, Pérez A, Pujol M. 1987. Experimental chemotherapy and toxicity in mice of three mebendazole polymorphic forms. Chemotherapy 33:266–271.

9. Martins FT, Neves PP, Ellena J, Camí GE, Brusau EV, Narda GE. 2009. Intermolecular contacts influencing the conformational and geometric features of the pharmaceutically preferred mebendazole polymorph C. J Pharm Sci 98:2336–2344.

10. Ferreira FF, Gutierrez Antonio S, Pires Rosa PC, de Oliveira Paiva-Santos C. 2010. Crystal structure determination of mebendazole form A using high-resolution synchrotron X-ray powder diffraction data. J Pharm Sci 99:1734–1744.
11. Evans AC, Fincham JE, Dhansay MA, Liebenberg W. 1999. Anthelmintic efficacy of mebendazole depends on the molecular polymorph. S Afr Med J 89:1118.
12. García-Rodriguez JJ, de la Torre-Iglesias PM, Vegas-Sánchez MC, Torrado-Durán S, Bolás-Fernández F, Torrado-Santiago S. 2011. Changed crystallinity of mebendazole solid dispersion: Improved anthelmintic activity. Int J Pharm 403:23–28.
13. Kawabata Y, Wada K, Nakatani M, Yamada S, Onoue S. 2011. Formulation design for poorly water-soluble drugs based on biopharmaceutics classification system: Basic approaches and practical applications. Int J Pharm 420:1–10.
14. Blaton NM, Peeters OM, De Ranter CJ. 1980. (5-Benzoyl-1H-benzimidazol-2-yl)-carbamic acid methyl ester hydrobromide (mebendazole·HBr), $C_{16}H_{14}BrN_3O_3$. Cryst Struct Commun 9:181–186.
15. Caira MR, Dekker TG, Liebenberg W. 1998. Structure of a 1:1 complex between the anthelmintic drug mebendazole and propionic acid. J Chem Crystallogr 28:11–15.
16. Brusau EV, Camí GE, Narda GE, Cuffini S, Ayala AP, Ellena J. 2008. Synthesis and characterization of a new mebendazole salt: Mebendazole hydrochloride. J Pharm Sci 97:542–552.
17. Chen J-M, Wang Z-Z, Wu CB, Li S, Lu T-B. 2012. Crystal engineering approach to improve the solubility of mebendazole. Cryst Eng Commun 14:6221–6229.
18. Kumar S, Chawla G, Sobhia ME, Bansal AK. 2008. Characterization of solid-state forms of mebendazole. Pharmazie 63:136–143.
19. Enraf-Nonius 1997–2000. COLLECT Nonius BV, Delft, The Netherlands.
20. Otwinowski Z, Minor W. 1997. Processing of X-ray diffraction data collected in oscillation mode. Methods Enzymol 276:307–326. Carter CW Jr, Sweet RM. Macromolecular Crystallography, Part A. New York: Academic Press.
21. Farrugia LJ. 2012. WinGXand ORTEP for Windows: an update. J Appl Cryst 32:837–838.
22. Farrugia LJ. 1997. ORTEP-3 for Windows—A version of ORTEP-III with a graphical user interface (GUI). J Appl Cryst 30:565–565.
23. Bruno IJ, Cole JC, Edgington PR, Kessler MK, Macrae CF, McCabe P, Pearson J, Taylor R. 2002. New software for searching the Cambridge Structural Database and visualizing crystal structures Acta Crystallogr B 58:389–397.
24. Allen FH, Johnson O, Shields GP, Smith BR, Towler M. 2004. CIF applications. XV. enCIFer: A program for viewing, editing and visualizing CIFs. J Appl Cryst 37:335–338.
25. Spek AL. 2001. PLATON—A multipurpose crystallographic tool. Ultrecht University, Ultrecht, The Netherlands.
26. Altomare A, Burla MC, Camalli M, Cascarazo GL, Giacovazzo C, Guagliardi A, Moliterni AGG, Polidori G, Spagna R. 1999. SIR97. J Appl Cryst 32:115–119.
27. Sheldrick GM. 2008. A short history of SHELX. Acta Crystallogr A 64:112–122.
28. Nardelli MJ. 1983. PARST: A system of fortran routines for calculating molecular structure parameters from results of crystal structure analyses. Comput Chem 7:95–97.
29. Nardelli MJ. 1995. PARST. Appl Cryst 28:659.
30. Coppens P, Leiserowitz L, Rabinovich D. 1965. Calculation of absorption corrections for camera and diffractometer data. Acta Cryst 18:1035–1038.
31. Bruno IJ, Cole JC, Kessler M, Luo J, Motherwell WDS, Purkis LH, Smith BR, Taylor R, Cooper RI, Harris SE, Orpen AG. 2004. Retrieval of crystallographically-derived molecular geometry information. J Chem Inf Comput Sci, 44:2133–2144.
32. Allen FH. 2002. The Cambridge Structural Database: A quarter of a million crystal structures and rising. Acta Crystallogr B 58:380–388.
33. Sirisuth N, Augsburger LL, Eddington ND. 2002. Development and validation of a non-linear IVIVC model for a diltiazem extended release formulation. Biopharm Drug Dispos 23:1–8.
34. Tang L, Khan SU, Muhammad NA. 2001. Evaluation and selection of bio-relevant dissolution media for a poorly water-soluble new chemical entity. Pharm Dev Technol 6:531–540.
35. Jamzad S, Fassihi R. 2006. Role of surfactant and pH on dissolution properties of fenofibrate and glipizide—A technical note. AAPS PharmSciTech 7(2):E33.
36. United States Pharmacopeia and National Formulary USP 29-NF 24. 2006. Rockville, Maryland: United States Pharmacopeia Convention, Inc.
37. Gilli G, Bellucci F, Ferretti V, Bertolasi V. 1989. Evidence for resonance-assisted hydrogen bonding from crystal–structure correlations on the enol form of the beta-diketone fragment. J Am Chem Soc 111:1023–1028.
38. Giacovazzo C, Monaco HL, Artioli G, Viterbo D, Milanesio M, Gilli G, Gilli P, Zanotti G, Ferraris G. 2006. Fundamentals of crystallography. New York: Oxford University Press.
39. Prestch E, Clerc T, Seibl J, Simon W. 1998. Tablas para la dilucidación estructural de compuestos orgánicos por métodos espectroscópicos: ^{13}CRMN, ^{1}H-RMN, IR, EM, UV–Vis. Barcelona, Spain: Singer Verlag-Ibérica.
40. Klots TD, Devlin P, Collier WB. 1997. Heteroatom derivatives of indene V. Vibrational spectra of benzimidazole 1. Spectrochim Acta A Mol Biomol Spectrosc 53:2445–2456.
41. Morsy MA, Al-Khaldi MA, Suwaiyan A. 2002. Normal vibrational mode analysis and assignment of benzimidazole by ab initio and density functional calculations and polarized infrared and Raman spectroscopy. J Phys Chem A 106:9196–9203.